Development of Coating Architectures to Prevent Molten Sand Degradation of Turbine Coatings

PURDUE UNIVERSITY
School of Materials Engineering

Riordan Boyle, Ryan Heavener, Robert Miller, Quentin Pitter
Faculty Advisor: Dr. Rodney Trice
Industrial Sponsors: Dr. Adam Chamberlain, Dr. Robert Golden, Dr. Stephanie Gong, Bill Jarosinski, Dr. Molly O'Connor

Thermal barrier coatings (TBCs) are used to thermally insulate metallic components of gas turbine engines. As efficiency standards increase, the increased operating temperatures have resulted in the TBCs being chemically attacked by molten sand known as CMAS (calcium-magnesium aluminosilicate). Gadolinium zirconate (GZO) coatings have been shown to have a fast chemical reaction with molten CMAS. Different GZO coatings were studied to identify important microstructural characteristics to prevent CMAS infiltration and protect the underlying Yttria-stabilized zirconia (YSZ) TBC.

This work is sponsored by Rolls-Royce and Praxair Surface Technologies

Project Background

Motivation: Yttria stabilized zirconia is a common thermal barrier coating used to protect the nickel-based superalloy blades in gas turbine engines. Due to increased operating temperatures in gas turbine engines, YSZ needs protection from calcium-magnesium aluminosilicate. CMAS degrades YSZ by destabilizing the zirconia phase. This phase transformation causes delamination of YSZ after repeated heating and cooling thermal cycles.

Solution: The topcoat of gadolinium zirconate will reduce CMAS infiltration into the YSZ coating. This multilayer ceramic system provides resistance to CMAS infiltration by enabling fast-reacting phase transformations. Different microstructures of GZO were provided by Praxair Surface Technologies using different variations of plasma spray methods such as atmospheric plasma spray (APS) and suspension plasma spray (SPS).

Project Goal: To conduct CMAS furnace testing on the surface of 1-inch GZO-coated button samples. SEM images will be taken after testing and XRD completed for each GZO coating that is intact after testing. After analysis, the trends and microstructural features will be determined to identify which coatings contribute to the preservation of the GZO and YSZ layers. Samples tested include five types of GZO microstructures deposited onto two different YSZ microstructures. Also, all data will be provided to the sponsors to contribute to further works to find suitable microstructures to combat CMAS infiltration.

Figure 1: Example of CMAS entering turbine engines.

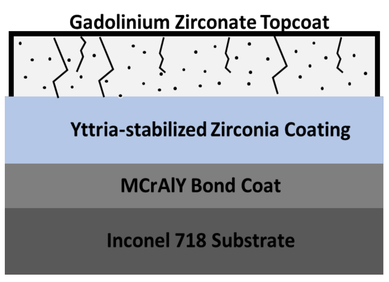

Figure 2: Schematic of coating layer structure.

Experimental Procedure

CMAS Application: Half-inch diameter CMAS tapes were centered on top of each sample, as shown in Figure 3, and inserted into the furnace. The temperature was increased at a rate of 10°C/min to 650°C to evaporate the adhesive tape, and then isothermally held for one hour. Next, the temperature was increased at the same rate to 1250°C, above the melting temperature for CMAS, and isothermally held for one hour. Finally, the samples were cooled to room temperature at a rate of 10°C/min. The weights of the samples were taken before and after the CMAS melting test to calculate CMAS loading.

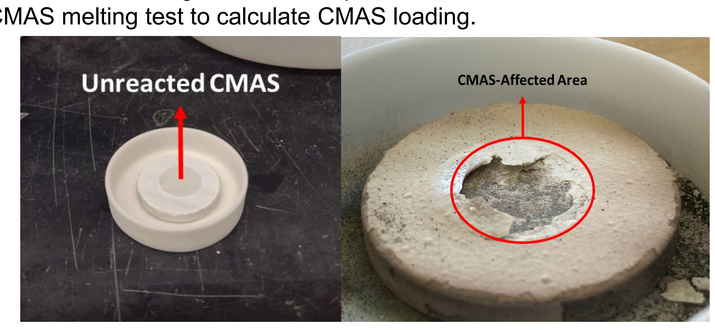

Figure 3: Before (left) and after (right) for a CMAS test on a sample.

Imaging Preparation: As-received samples were sectioned using a low-speed diamond saw and mounted using an 8-hour cure epoxy. CMAS tested samples were mounted first to protect the infiltrated GZO layer. Next, they were sectioned and re-mounted. Each mounted sample was polished at a plate speed of 300 rpm from 320 grit to 1-micron diamond paste.

SEM + EDS: SEM images were taken of the sample cross sections at 500x, 1000x, and 2000x magnification. EDS was used to conduct line scans through the cross section to map CMAS infiltration within the coating layers.

Microstructural Analysis: Analysis of the microstructures was conducted on the SEM images using ImageJ. Coating thickness and other one-dimensional measurements were measured by hand in the program. Area measurements were measured using a greyscale threshold and the particle analysis function of the program (Figure 4).

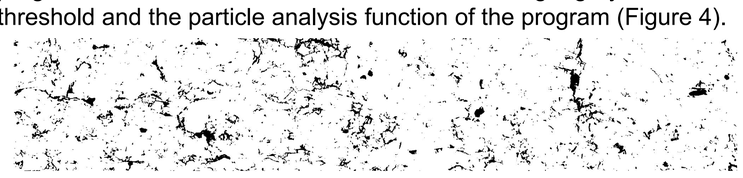

Figure 4: ImageJ greyscale threshold analysis example image.

Table 1: Microstructural characterization results for each sample.

Sample	As-Received Microstructure		As-Received Coating Thickness (μm)		Percent Porosity (%)		Percent Crack Area (%)		Percent Delamanated Area (%)	Average Remaining Coating Percent (%)	Layer of Delamination
	GZO	YSZ	GZO	YSZ	GZO	YSZ	GZO	YSZ			
A	APS DVC 1	APS DVC	187	144	2.5	4.4	2.3	3.1	N/A	23.4% YSZ	Majority YSZ
B	APS DVC 2	APS DVC	142	148	3.5	4.5	2.0	3.0	71	18.8% YSZ	Majority YSZ
C	APS DVC 3	APS DVC	119	149	4.3	4.1	1.0	1.9	0	48.4% GZO	Partial GZO
D	SPS DVC 4	APS DVC	132	141	1.1	3.5	0.9	3.0	29	20.8% YSZ	Majority YSZ
E	SPS DVC 5	APS DVC	128	141	4.4	3.4	2.8	1.1	46	18.7% YSZ	Majority YSZ
F	APS DVC 1	SPS Columnar	178	168	1.1	5.4	1.1	11.8	72	19.3% YSZ	Majority YSZ
G	APS DVC 2	SPS Columnar	154	170	2.1	6.1	0.5	11.5	36	16% YSZ	Majority YSZ
H	APS DVC 3	SPS Columnar	143	159	2.5	5.4	0.6	14.6	0	70.1% GZO	Partial GZO
I	SPS DVC 5	SPS Columnar	127	179	3.1	5.9	4.8	13.3	0	5.62% GZO	GZO/YSZ Interface
J	SPS DVC 4	SPS Columnar	130	158	1.6	5.1	0.2	15.8	N/A	37.7% GZO	Partial GZO

Results & Discussion

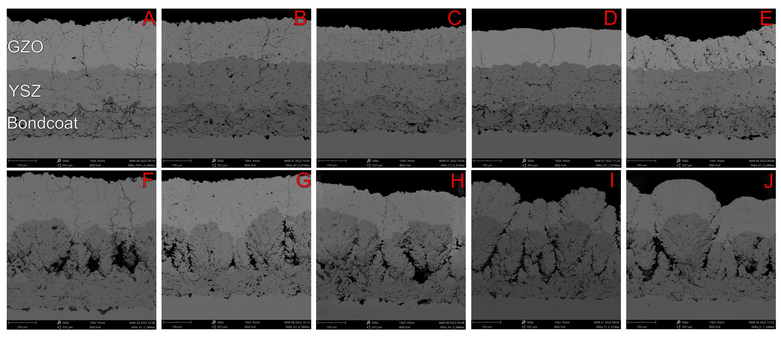

Figure 5: A collage of all as-received microstructures. Samples are labeled A-J.

SEM images of the as-received samples revealed differences in microstructures based on different plasma spray methods and spray conditions. From Table 1, samples with SPS columnar YSZ microstructures had greater percent porosities and percent crack areas compared to APS DVC YSZ microstructures. Observationally, APS DVC GZO microstructures had uniform dispersion of porosity and cracks (Figure 5). APS DVC 3 GZO had the highest percent porosity and lowest percent crack area compared to APS DVC 1 and APS DVC 2 GZO microstructures. SPS DVC 4 GZO had lower percent porosity and percent crack area than SPS DVC 5 GZO (Table 1).

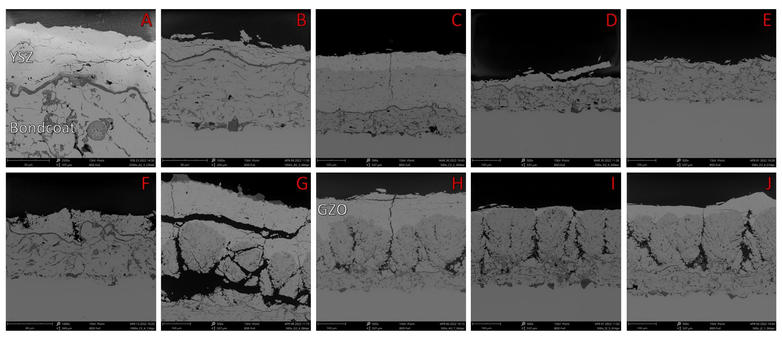

Figure 6: A collage of all samples after CMAS testing. Samples are labeled A-J.

EDS compositional data revealed that all samples were subjected to complete infiltration of both the GZO and YSZ layers. This may have been due to higher experimental CMAS loading or lack of a thermal gradient between coating layers. Therefore, no determination can be made for which GZO coating microstructure exhibited the most resistance to CMAS infiltration.

The success of the samples was determined by the depth of delamination that occurred after CMAS testing and the average remaining coating percentage. Samples A, B, D, E, F, and G exhibited nearly complete spallation to the bottom of the YSZ layer. Therefore, these coatings performed poorly due to less thermomechanical stability. Samples C, H, and J exhibited partial spallation of the GZO layer (Figure 6). These coatings had the best performance due to more thermomechanical stability. Sample I had performed moderately, spalling at the GZO/YSZ interface.

Table 2: Sub-table ranking each sample by the ratio of GZO porosity to crack area.

Sample	GZO Microstructure	GZO Porosity/Crack Area Ratio	Layer of Delamination
J	SPS DVC 4	7.6	Partial GZO
C	APS DVC 3	4.5	Partial GZO
G	APS DVC 2	4.4	Majority YSZ
H	APS DVC 3	4.2	Partial GZO
B	APS DVC 2	1.7	Majority YSZ
E	SPS DVC 5	1.6	Majority YSZ
D	SPS DVC 4	1.3	Majority YSZ
A	APS DVC 1	1.1	Majority YSZ
F	APS DVC 1	1.0	Majority YSZ
I	SPS DVC 5	0.6	GZO/YSZ Interface

Table 2 shows that samples C, H, and J had greater GZO porosity to crack area ratios, which allowed for greater strain compliance for thermal expansion and resulted in better performance. Although sample G had a similar ratio value, the spray conditions for APS DVC 2 GZO resulted in complete spallation for both coatings.

Results & Discussion Cont.

Table 3: Sub-table outlining the YSZ percent porosity and percent crack area.

Sample	YSZ Microstructure	YSZ Percent Porosity (%)	YSZ Percent Crack Area (%)	Layer of Delamination
A	APS DVC	4.4	3.1	Majority YSZ
B	APS DVC	4.5	3.0	Majority YSZ
C	APS DVC	4.1	1.9	Partial GZO
D	APS DVC	3.5	3.0	Majority YSZ
E	APS DVC	3.4	1.1	Majority YSZ
F	SPS Columnar	5.4	11.8	Majority YSZ
G	SPS Columnar	6.1	11.5	Majority YSZ
H	SPS Columnar	5.4	14.6	Partial GZO
I	SPS Columnar	5.9	13.3	GZO/YSZ Interface
J	SPS Columnar	5.1	15.8	Partial GZO

Samples A, B, D, and E all performed poorly due to the effect of the APS DVC YSZ microstructure on the overall strain compliance of the coatings. This is due to the higher density of the APS DVC YSZ microstructure that decreases the strain compliance of the coatings. APS DVC 3 GZO (samples C and H) spray conditions resulted in favorable thermomechanical stability (Table 3).

The underlying YSZ microstructure had a measurable effect on the formation of GZO topcoat. This is evident in both the performance and overall structure of the coatings. SPS columnar YSZ microstructures resulted in lower GZO percent crack area for all coatings besides SPS DVC 5 (Table 3). Samples H, I , and J performed well due to this interaction whereas samples F and G did not due to the unfavorable GZO spray conditions (APS DVC 1 and APS DVC 2).

Summary and Recommendations

Based on the results, the CMAS loading was higher than expected. One contributing factor is the surface roughness of the GZO which prevents the CMAS to spread when molten. Also, there was no thermal gradient to replicate interior cooling that occurs naturally. Instead of only the surface being heated, the entire sample was heated uniformly.

For future works, we recommend an experiment that compares CMAS infiltration depth at shorter isothermal holds with the presence of a thermal gradient. We predict that this would allow some GZO coatings to prevent complete infiltration. Also, we recommend another experiment that tests how thermal cycles for set intervals of time affect the mechanical properties of each microstructure.

References

- Kumar, R., Jordan, E., Gell, M., Roth, J., Jiang, C., Wang, J., & Rommel, S. (2017). CMAS behavior of Yttrium Aluminum Garnet (YAG) and yttria-stabilized zirconia (Ysz) thermal barrier coatings. *Surface and Coatings Technology*, *327*, 126–138.
- Shifler, D. A., & Choi, S. R. (2018). CMAS effects on ship gas-turbine components/materials. *Volume 1: Aircraft Engine; Fans and Blowers; Marine.*
- Golden, R. (2021). *CMAS Tape Fabrication and Loading Procedure.*
- Levi, C.G., Hutchinson, J.W., Vidal-Sétif, (2012).Environmental degradation of thermal-barrier coatings by molten deposits. *MRS Bulletin* **37,** 932–941
- Krämer, S., Yang, J., Levi, C.G. and Johnson, C.A. (2006), Thermochemical Interaction of Thermal Barrier Coatings with Molten CaO–MgO–Al2O3–SiO2 (CMAS) Deposits. Journal of the American Ceramic Society, 89: 3167-3175.

Acknowledgements

We would like to express our gratitude to our industry sponsors from Rolls-Royce: Dr. Adam L. Chamberlain, Dr. Robert Golden and Dr. Stephanie Gong and Praxair Surface Technologies: Dr. Molly O'Connor and William Jarosinski, whose continuous cooperation and support made our efforts worthwhile. We would also like to thank our faculty advisor, Dr. Rodney W. Trice, who offered endless motivation and wisdom for the duration of the project.

MSE 430 - 440: Materials Processing and Design